Immobilized Co-Bis(benzenedithiolate) Complexes: Exceptionally Active Heterogeneous Electrocatalysts for Dihydrogen Production from Mildly Acidic Aqueous Solutions

Shawn C. Eady, Molly M. MacInnes, and Nicolai Lehnert*

Department of Chemistry, University of Michigan,930 North University Ave, Ann Arbor, MI 48109
Email: lehnertn@umich.edu

Supporting Information

Table of Contents.

1. UV-Visible Spectroscopy
    a. **Figure S1.** UV-Visible spectra of cobalt-bis(benzenedithiolate) complexes in dichloromethane solution.
2. X-ray Photoelectron Spectroscopy
    a. **Figure S2.** (TBA)[$Co(S_2C_6Cl_4)_2$] (**3**) adsorbed on a FTO/RGO electrode.
    b. **Figure S3.** (TBA)[$Co(S_2C_{10}H_6)_2$] (**6**) adsorbed on a FTO/RGO electrode.
    c. **Figure S4.** (TBA)[$Co(S_2C_6Cl_2)_2$] (**2**) adsorbed on a HOPG electrode
3. Electrochemical Measurements
    a. **Figure S5.** Cyclic voltammetry of RGO-coated FTO.
    b. **Figure S6.** Cyclic voltammetry of (TBA)[$Co(S_2C_6H_4)_2$] (**1**) adsorbed on a FTO/RGO working electrode at various scan rates.
    c. **Figure S7.** Cyclic voltammetry of (TBA)[$Co(S_2C_6H_4)_2$] (**1**) adsorbed on a FTO/RGO working electrode with addition of TFA.
    d. **Figure S8.** Cyclic voltammograms of (TBA)[$Co(S_2C_6H_4)_2$] (**1**) adsorbed on an HOPG working electrode in consecutively applied solutions in the absence and presence of acid.
    e. **Figure S9.** Cyclic voltammetry of (TBA)[$Co(S_2C_6Cl_2)_2$] (**2**) adsorbed on an HOPG working electrode at various scan rates.
    f. **Figure S10.** Cyclic voltammetry of (TBA)[$Co(S_2C_6Cl_4)_2$] (**3**) adsorbed on a FTO/RGO working electrode at various scan rates.
    g. **Figure S11.** Cyclic voltammetry of (TBA)[$Co(S_2C_6Cl_4)_2$] (**3**) adsorbed on a FTO/RGO working electrode with addition of TFA.
    h. **Figure S12.** Cyclic voltammetry of (TBA)[$Co(S_2C_6Cl_4)_2$] (**3**) adsorbed on an HOPG working electrode at various scan rates.
    i. **Figure S13.** Cyclic voltammograms of (TBA)[$Co(S_2C_6Cl_4)_2$] (**3**) adsorbed on HOPG and FTO/graphene working electrodes for comparison of overpotentials.
    j. **Figure S14.** Cyclic voltammetry of (TBA)[$Co(S_2C_6F_4)_2$] (**4**) adsorbed on a FTO/RGO working electrode at various scan rates.
    k. **Figure S15.** Cyclic voltammetry of (TBA)[$Co(S_2C_6F_4)_2$] (**4**) adsorbed on a FTO/RGO working electrode with addition of TFA.
    l. **Figure S16.** Cyclic voltammetry of (TBA)[$Co(S_2C_6F_4)_2$] (**4**) adsorbed on an HOPG working electrode at various scan rates.

m. **Figure S17** Cyclic voltammetry of (TBA)[$Co(S_2C_6F_4)_2$] (**4**) adsorbed on an HOPG working electrode with addition of TFA.
n. **Figure S18** Cyclic voltammetry of (TBA)[$Co(S_2C_7H_6)_2$] (**5**) adsorbed on a FTO/RGO working electrode at various scan rates.
o. **Figure S19** Cyclic voltammetry of (TBA)[$Co(S_2C_7H_6)_2$] (**5**) adsorbed on two distinct FTO/RGO working electrodes with addition of TFA.
p. **Figure S20** Cyclic voltammetry of (TBA)[$Co(S_2C_7H_6)_2$] (**5**) adsorbed on an HOPG working electrode at various scan rates.
q. **Figure S21** Cyclic voltammetry of (TBA)[$Co(S_2C_{10}H_6)_2$] (**6**) adsorbed on a FTO/RGO working electrode at various scan rates.
r. **Figure S22** Cyclic voltammetry of (TBA)[$Co(S_2C_{10}H_6)_2$] (**6**) adsorbed on a FTO/RGO working electrode with addition of TFA.
s. **Figure S23** Cyclic voltammetry of (TBA)[$Co(S_2C_{10}H_6)_2$] (**6**) adsorbed on an HOPG working electrode with addition of TFA.
t. **Figure S24** Controlled Potential Electrolysis at -0.5 V vs. SHE of (TBA)[$Co(S_2C_6Cl_4)_2$] (**3**) adsorbed to a HOPG electrode at pH 0.3.
u. **Figure S25** Cyclic voltammogram of (TBA)[$Co(S_2C_6Cl_4)_2$] (**3**) adsorbed to an HOPG electrode after CPE experiment in a new pH 7 electrolyte solution.
v. **Figure S26** Cyclic Voltammetry of (TBA)[$Co(S_2C_6Cl_2)_2$] (**2**) adsorbed on a rough HOPG working electrode to demonstrate acid stability over time

4. Determination of Catalytic Turnover Frequencies
    a. Acid titration cyclic voltammetry experiments
    b. Bulk electrolysis
5. X-ray crystallography
    a. **Table S1.** Crystal data and structure refinement for **6**.
6. References

1. UV-Visible Spectroscopy

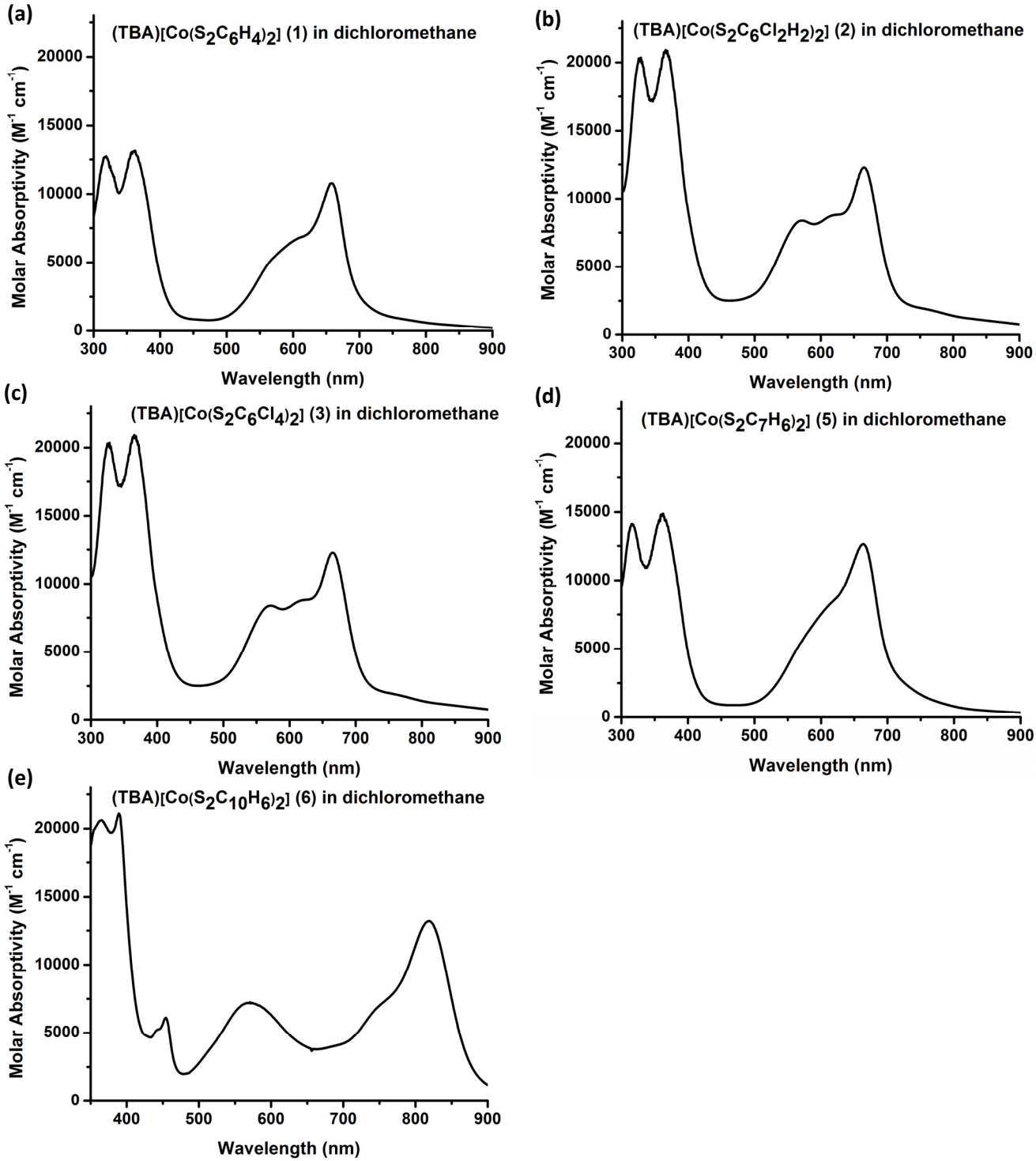

Figure S1. UV-Visible spectra (in dichloromethane solution) of (a) (TBA)[$Co(S_2C_6H_4)_2$] (**1**); (b) (TBA)[$Co(S_2C_6Cl_2H_2)_2$] (**2**); (c) (TBA)[$Co(S_2C_6Cl_4)_2$] (**3**); (d) (TBA)[$Co(S_2C_7H_6)_2$] (**5**); and (e) (TBA)[$Co(S_2C_{10}H_6)_2$] (**6**).

2. X-ray Photoelectron Spectroscopy

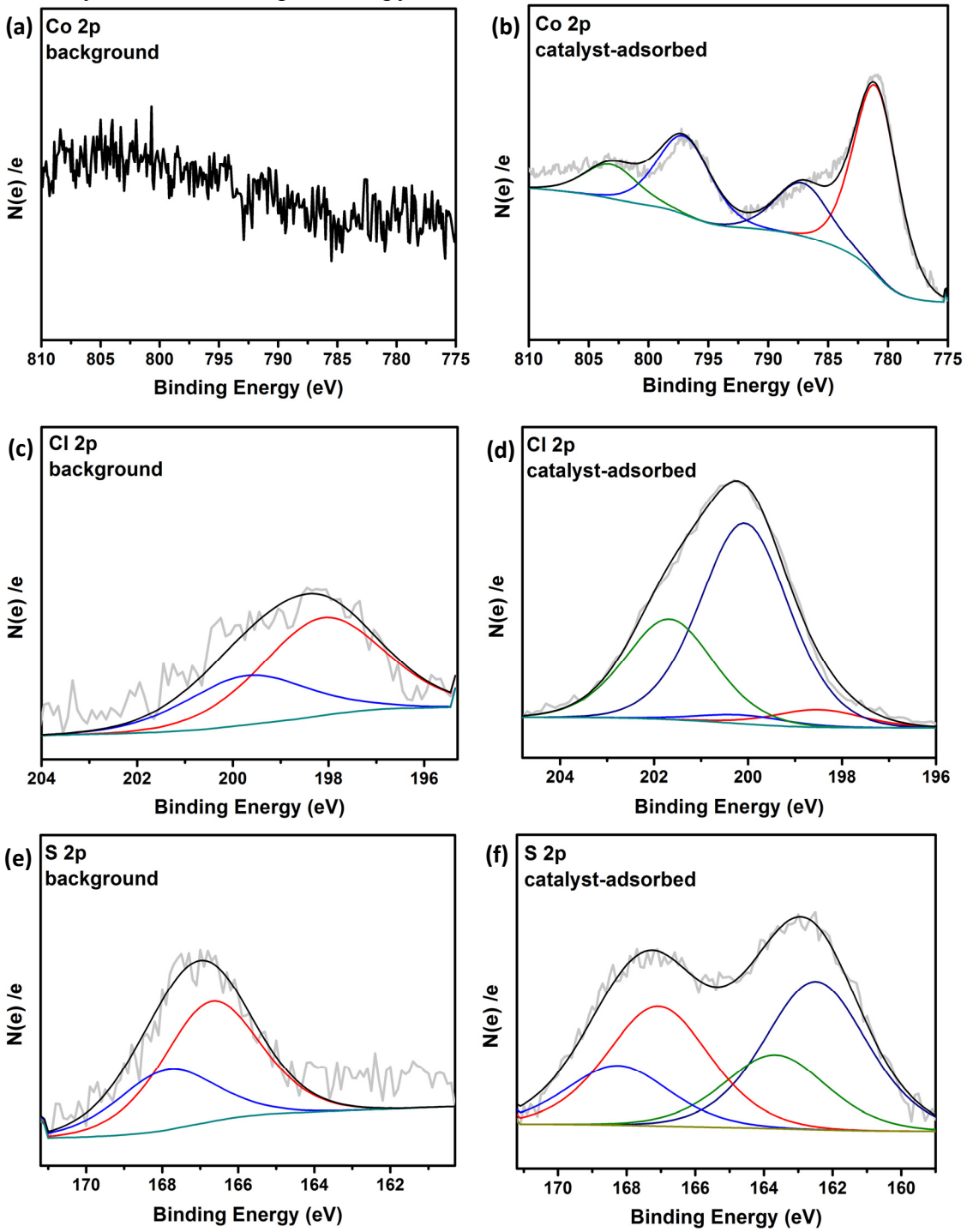

Figure S2. X-ray photoelectron spectroscopy (XPS) analysis of TBA[$Co(S_2C_6Cl_4)_2$] (**3**) on a FTO/RGO electrode. (a) background Co 2p core level XPS spectrum of bare FTO/RGO; (b) Co 2p core level XPS spectrum of catalyst-adsorbed FTO/RGO; (c) background Cl 2p core level XPS spectrum of bare FTO/RGO; (d) Cl 2p core level XPS spectrum of catalyst-adsorbed FTO/RGO; (e) background S 2p core level XPS spectrum of bare FTO/RGO; (f) S 2p core level XPS spectrum of catalyst-adsorbed FTO/RGO. The envelope is included as a solid black trace.

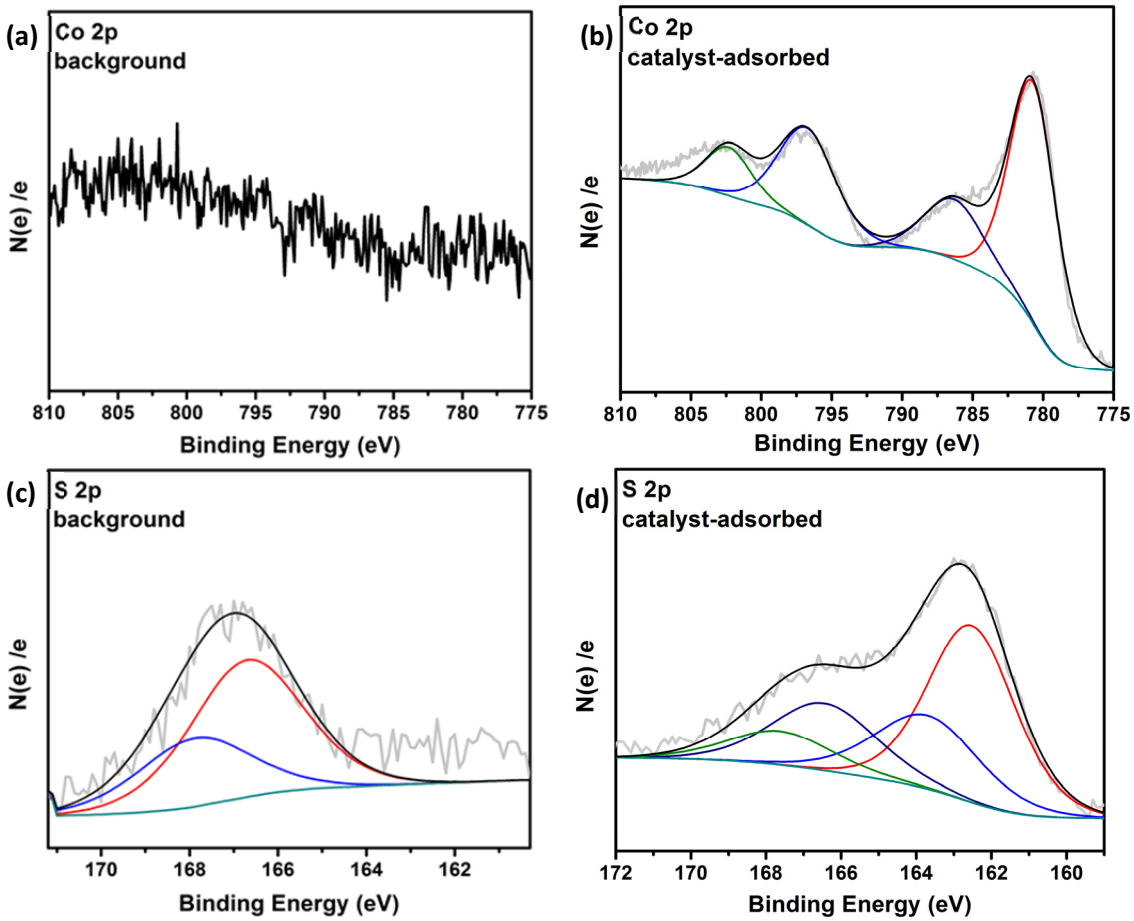

Figure S3. X-ray photoelectron spectroscopy (XPS) analysis of TBA[$Co(S_2C_{10}H_6)_2$] (**6**) on a FTO/RGO electrode. (a) background Co 2p core level XPS spectrum of bare FTO/RGO; (b) Co 2p core level XPS spectrum of catalyst-adsorbed FTO/RGO; (c) background S 2p core level XPS spectrum of bare FTO/RGO; (d) S 2p core level XPS spectrum of catalyst-adsorbed FTO/RGO. The envelope is included as a solid black trace.

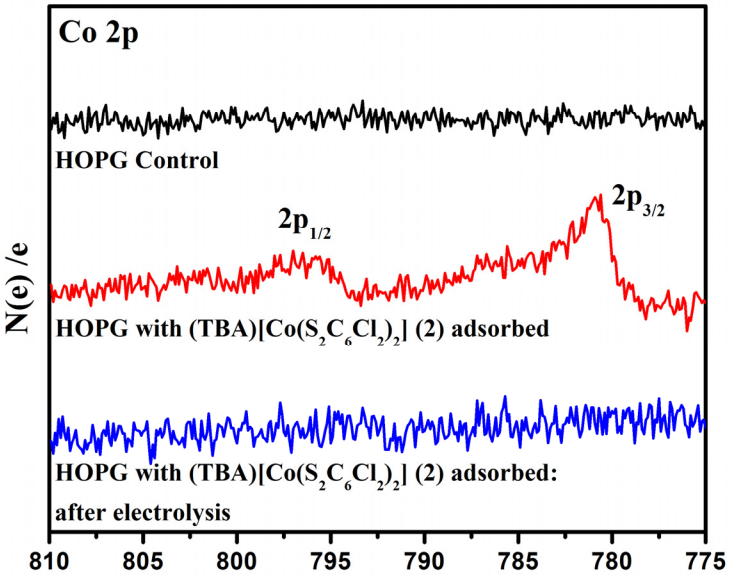

Figure S4. X-ray photoelectron spectroscopy (XPS) analysis of (TBA)[$Co(S_2C_6Cl_2H_2)_2$] (**2**) on a HOPG electrode before and after electrolysis at -0.5 V vs. SHE in an aqueous 0.1 M KPF_6 solution with 0.5 M H_2SO_4 (pH 0.3).

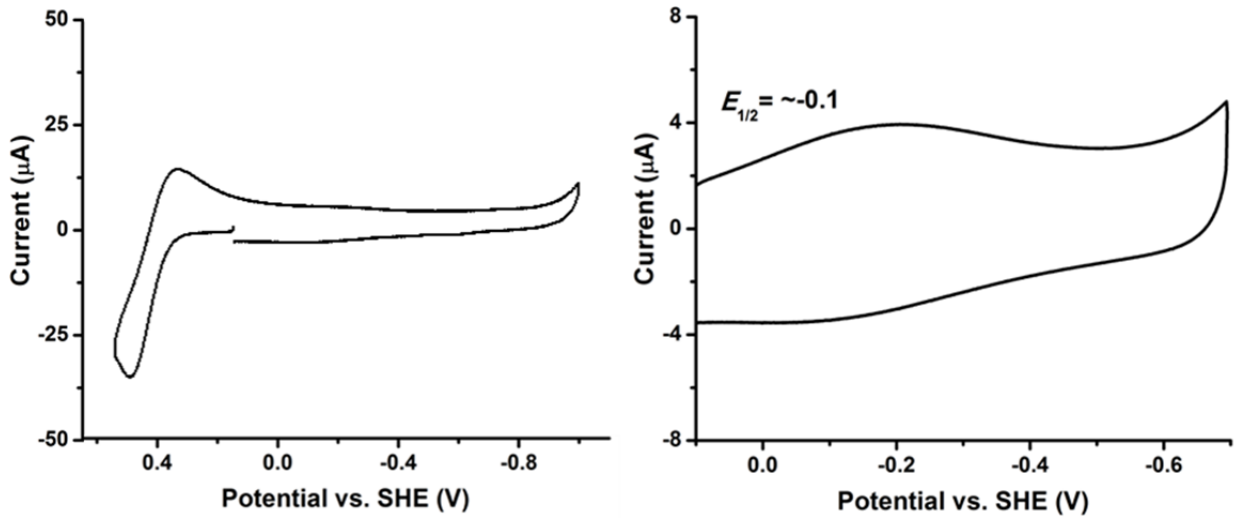

Figure S5. *Left:* Electrochemical window of RGO-coated FTO in aqueous 0.1 M potassium hexafluorophosphate with potassium ferricyanide/ferrocyanide (0.5 mM total) as the internal reference. *Right:* Zoomed view of the cathodic window to show the background signal for FTO/RGO electrodes. The scan rate was 50 mV/s. Potentials reported are versus the standard hydrogen electrode (SHE).

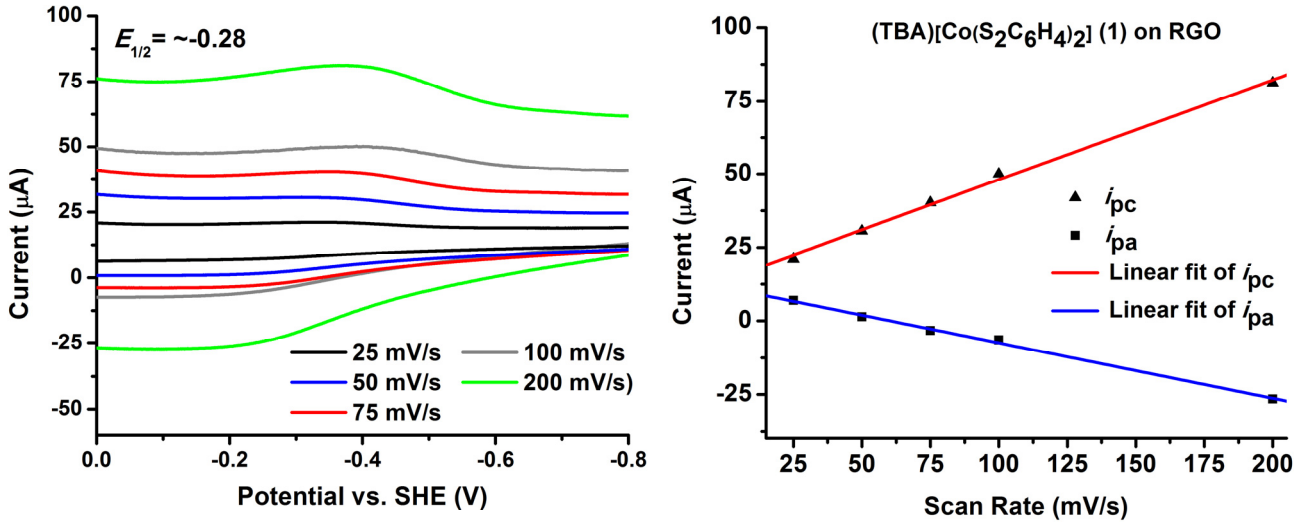

Figure S6. *Left:* Cyclic voltammetry of (TBA)[$Co(S_2C_6H_4)_2$] (**1**) adsorbed on a **FTO/RGO** working electrode at various scan rates. The solution contained 0.1 M aqueous potassium hexafluorophosphate. The counter electrode was a platinum disc, and the reference was an Ag/AgCl (saturated KCl solution) electrode. An equimolar solution of potassium ferricyanide/ferrocyanide (0.5 mM total) was used as an external standard. Potentials are reported versus the standard hydrogen electrode. *Right:* Linear fit of the peak cathodic and anodic current versus the scan rate.

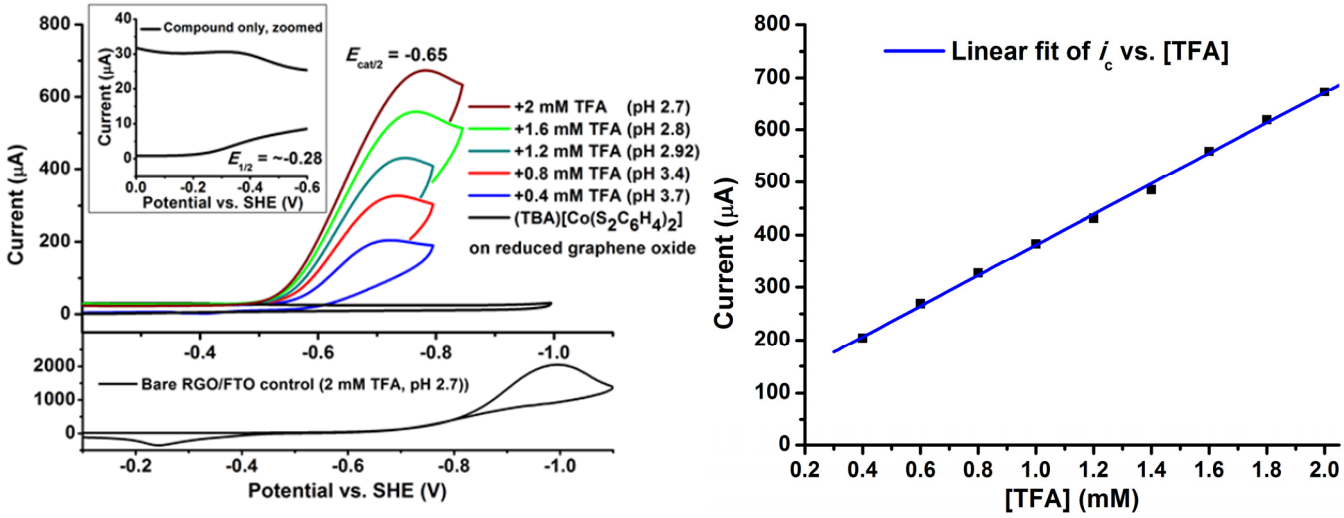

Figure S7. *Left:* Cyclic voltammetry of (TBA)[Co($S_2C_6H_4$)$_2$] (**1**) adsorbed on a **FTO/RGO** working electrode with addition of TFA at a scan rate of 50 mV/s. The control surface (using an FTO/RGO electrode without adsorbed catalyst) under the same conditions is displayed on the bottom of the graph, and the inset provides a zoomed view of the CV of the Co catalyst functionalized surface in the absence of acid. The solution contained 0.1 M aqueous potassium hexafluorophosphate. The counter electrode was a platinum disc, and the reference was an Ag/AgCl (saturated KCl solution) electrode. An equimolar solution of potassium ferricyanide/ferrocyanide (0.5 mM total) was used as an external standard. Potentials are reported versus the standard hydrogen electrode. *Right:* Linear fit of the peak catalytic current versus increasing TFA concentrations, indicating an acid-diffusion controlled process under these conditions.

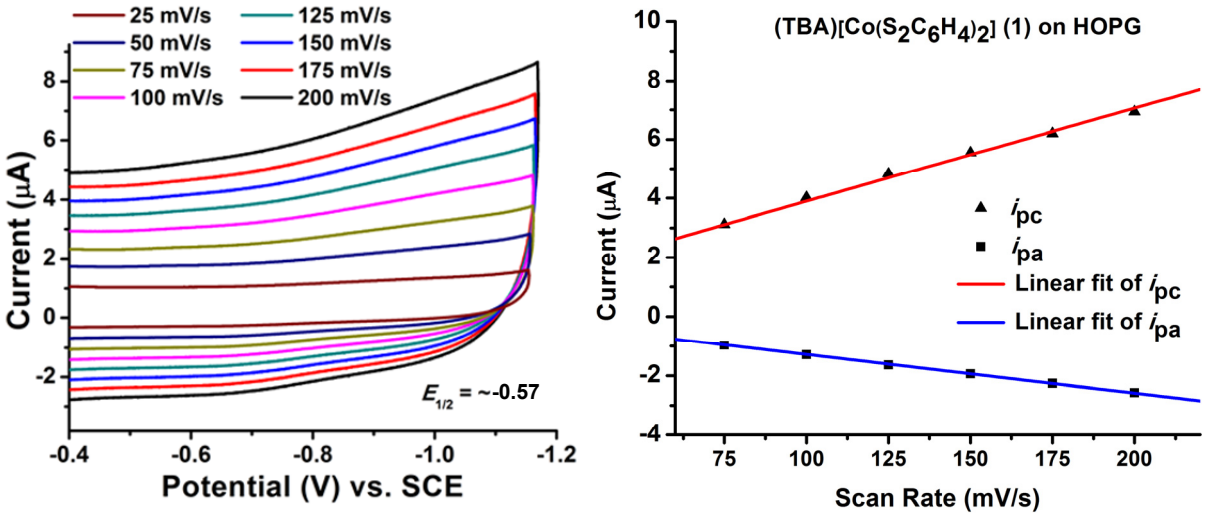

Figure S8. *Left:* Cyclic voltammetry of (TBA)[Co($S_2C_6H_4$)$_2$] (**1**) adsorbed on an **HOPG** working electrode at various scan rates. The solution contained 0.1 M aqueous potassium hexafluorophosphate. The counter electrode was a platinum disc, and the reference was an Ag/AgCl (saturated KCl solution) electrode. An equimolar solution of potassium ferricyanide/ferrocyanide (0.5 mM total) was used as an external standard. Potentials are reported versus the standard hydrogen electrode. *Right:* Linear fit of the peak cathodic and anodic current versus the scan rate.

.

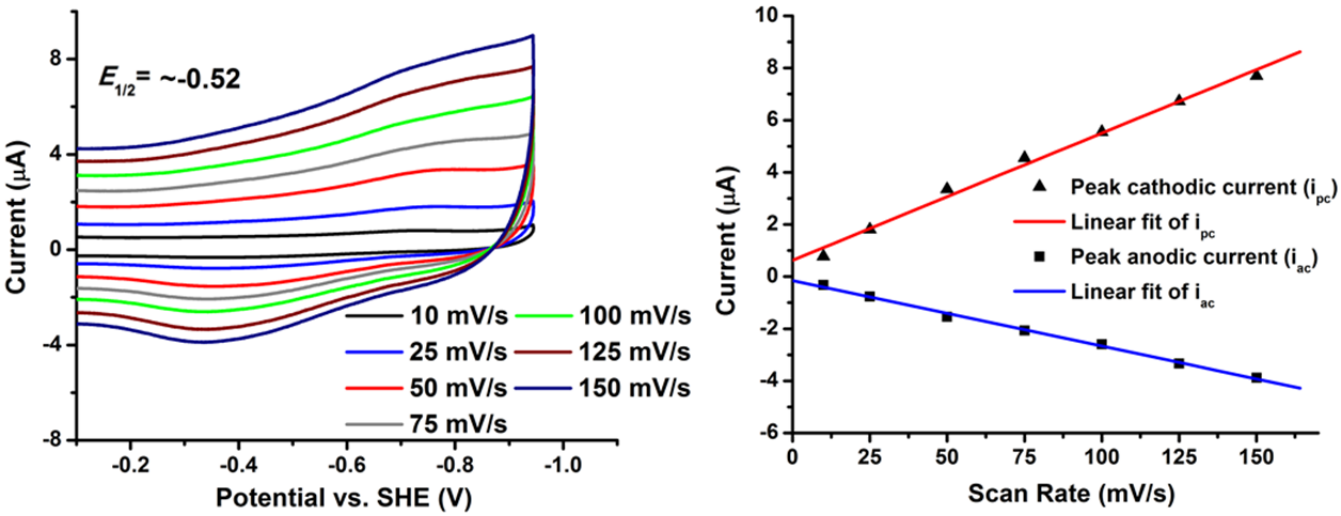

Figure S9. *Left:* Cyclic voltammetry of (TBA)[Co($S_2C_6Cl_2H_2$)$_2$] (**2**) adsorbed on an **HOPG** working electrode at various scan rates. The solution contained 0.1 M aqueous potassium hexafluorophosphate. The counter electrode was a platinum disc, and the reference was an Ag/AgCl (saturated KCl solution) electrode. An equimolar solution of potassium ferricyanide/ferrocyanide (0.5 mM total) was used as an external standard. Potentials are reported versus the standard hydrogen electrode. *Right:* Linear fit of the peak cathodic and anodic current versus the scan rate.

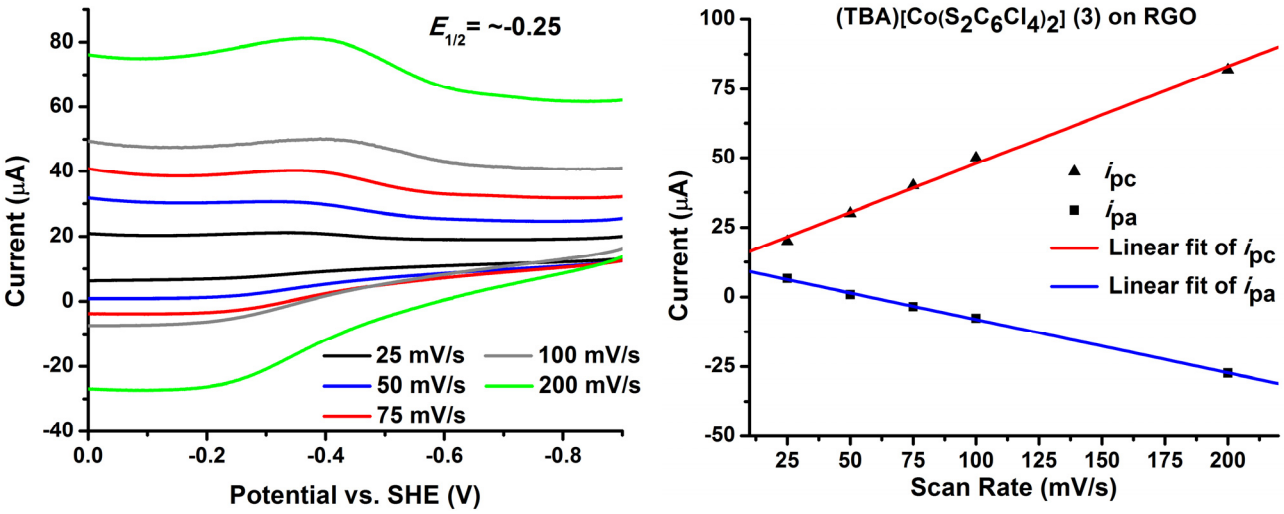

Figure S10. *Left:* Cyclic voltammetry of (TBA)[Co($S_2C_6Cl_4$)$_2$] (**3**) adsorbed on a **FTO/RGO** working electrode at various scan rates. The solution contained 0.1 M aqueous potassium hexafluorophosphate. The counter electrode was a platinum disc, and the reference was an Ag/AgCl (saturated KCl solution) electrode. An equimolar solution of potassium ferricyanide/ferrocyanide (0.5 mM total) was used as an external standard. Potentials are reported versus the standard hydrogen electrode. *Right:* Linear fit of the peak cathodic and anodic current versus the scan rate.

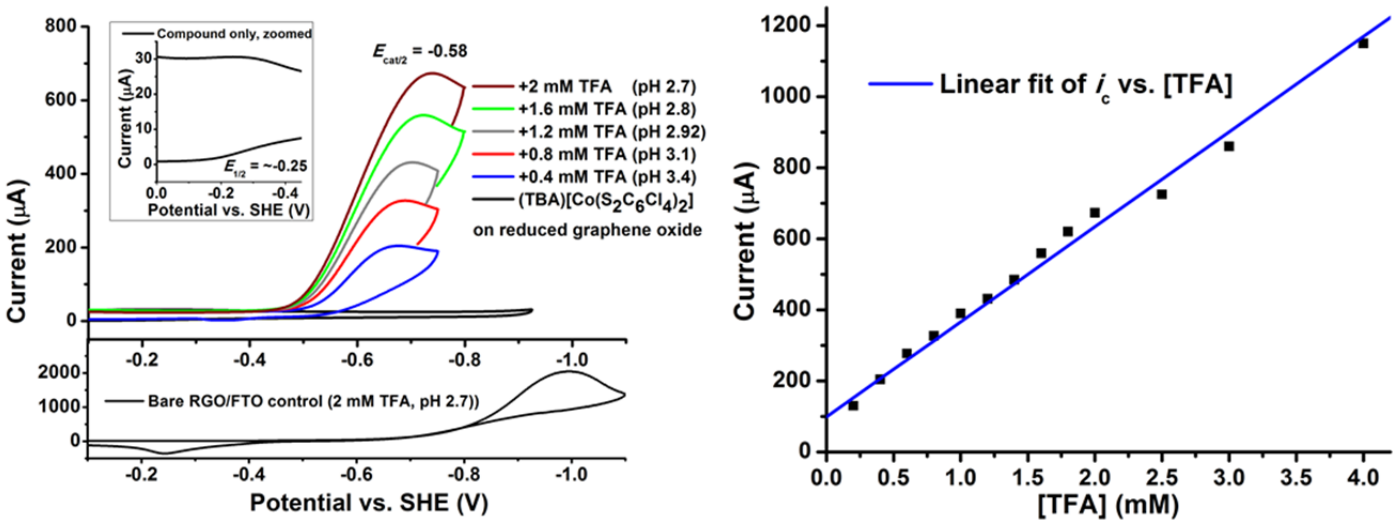

Figure S11. *Left:* Cyclic voltammetry of (TBA)[Co($S_2C_6Cl_4$)$_2$] (**3**) adsorbed on a **FTO/RGO** working electrode with addition of TFA at a scan rate of 50 mV/s. The control surface (using an FTO/RGO electrode without adsorbed catalyst) under the same conditions is displayed on the bottom of the graph, and the inset provides a zoomed view of the CV of the Co catalyst functionalized surface in the absence of acid. The solution contained 0.1 M aqueous potassium hexafluorophosphate. The counter electrode was a platinum disc, and the reference was an Ag/AgCl (saturated KCl solution) electrode. An equimolar solution of potassium ferricyanide/ferrocyanide (0.5 mM total) was used as an external standard. Potentials are reported versus the standard hydrogen electrode. *Right:* Linear fit of the peak catalytic current versus increasing TFA concentrations, indicating an acid-diffusion controlled process under these conditions.

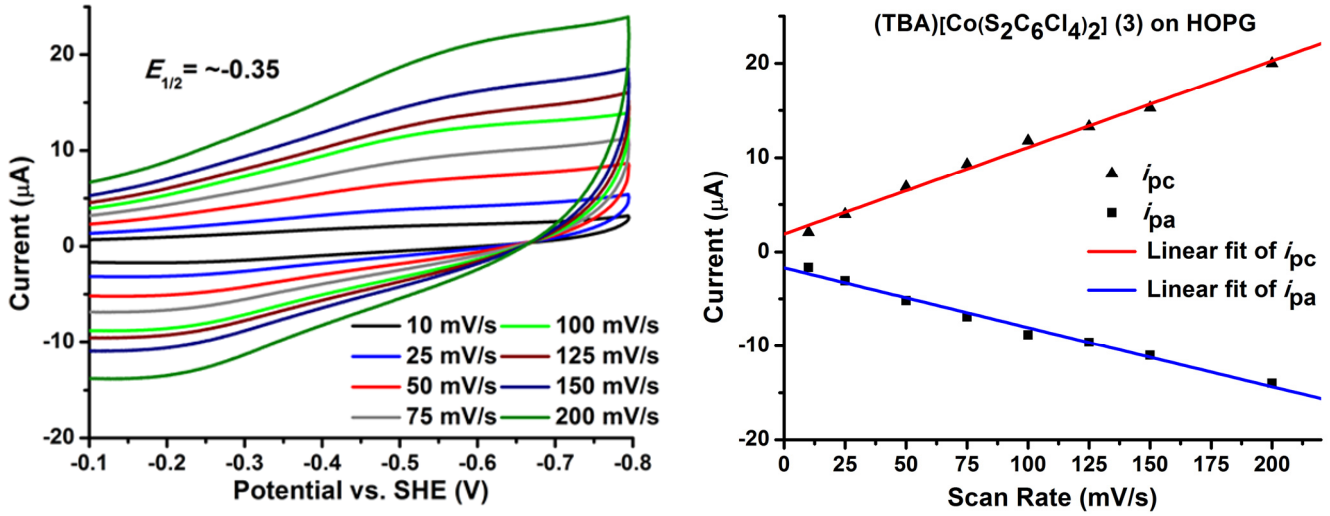

Figure S12. *Left:* Cyclic voltammetry of (TBA)[Co($S_2C_6Cl_4$)$_2$] (**3**) adsorbed on an **HOPG** working electrode at various scan rates. The solution contained 0.1 M aqueous potassium hexafluorophosphate. The counter electrode was a platinum disc, and the reference was an Ag/AgCl (saturated KCl solution) electrode. An equimolar solution of potassium ferricyanide/ferrocyanide (0.5 mM total) was used as an external standard. Potentials are reported versus the standard hydrogen electrode. *Right:* Linear fit of the peak cathodic and anodic current versus the scan rate.

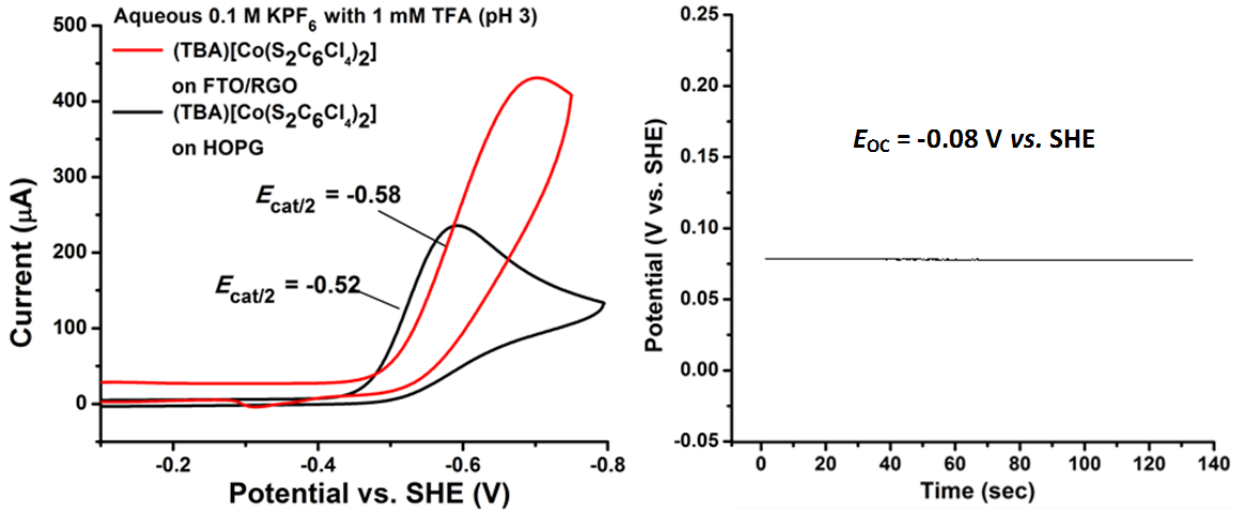

Figure S13. *Left:* Cyclic voltammetry of (TBA)[$Co(S_2C_6Cl_4)_2$] (**3**) adsorbed on **FTO/RGO** and **HOPG** working electrodes in a 1 mM TFA solution with a 50 mV/s scan rate as a representation of how overpotentials were determined for catalyst-adsorbed electrode systems, i.e. $\boldsymbol{\eta = E_{cat/2} - E_{OC}}$. *Right:* Open circuit potential over time of a platinum mesh working electrode in the same acid solution under 1 atm H_2 atmosphere to indicate overpotential. The solution contained 0.1 M aqueous potassium hexafluorophosphate. The counter electrode was a platinum wire, and the reference was an Ag/AgCl (saturated KCl solution) electrode. An equimolar solution of potassium ferricyanide/ferrocyanide (0.5 mM total) was used as an external reference. Potentials are reported versus the standard hydrogen electrode.

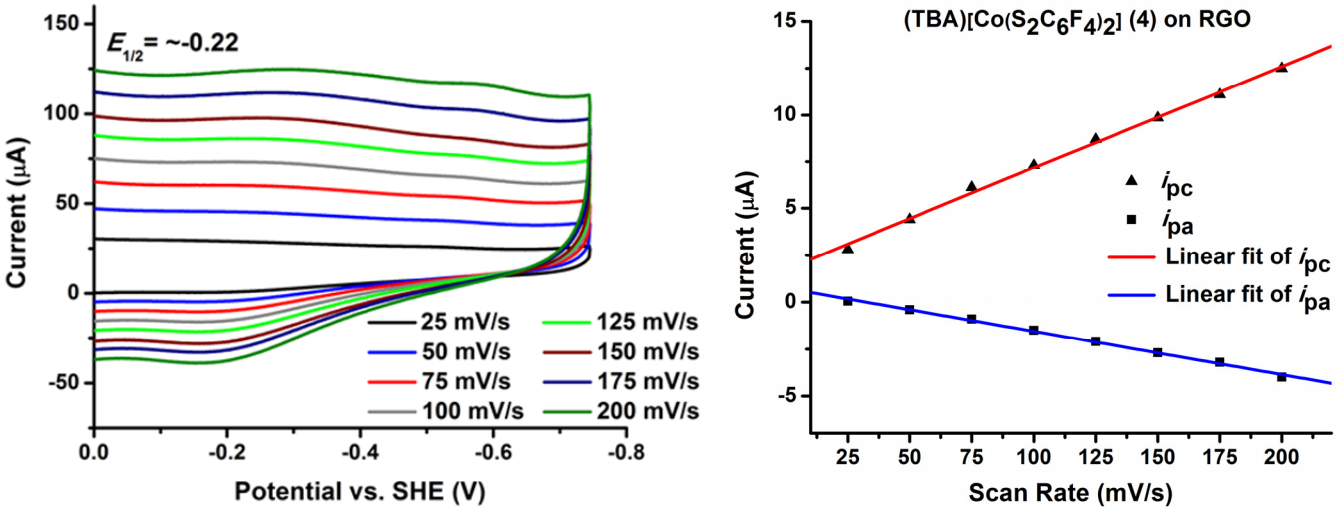

Figure S14. *Left:* Cyclic voltammetry of (TBA)[$Co(S_2C_6F_4)_2$] (**4**) adsorbed on a **FTO/RGO** working electrode at various scan rates. The solution contained 0.1 M aqueous potassium hexafluorophosphate. The counter electrode was a platinum disc, and the reference was an Ag/AgCl (saturated KCl solution) electrode. An equimolar solution of potassium ferricyanide/ferrocyanide (0.5 mM total) was used as an external standard. Potentials are reported versus the standard hydrogen electrode. *Right:* Linear fit of the peak cathodic and anodic current versus the scan rate.

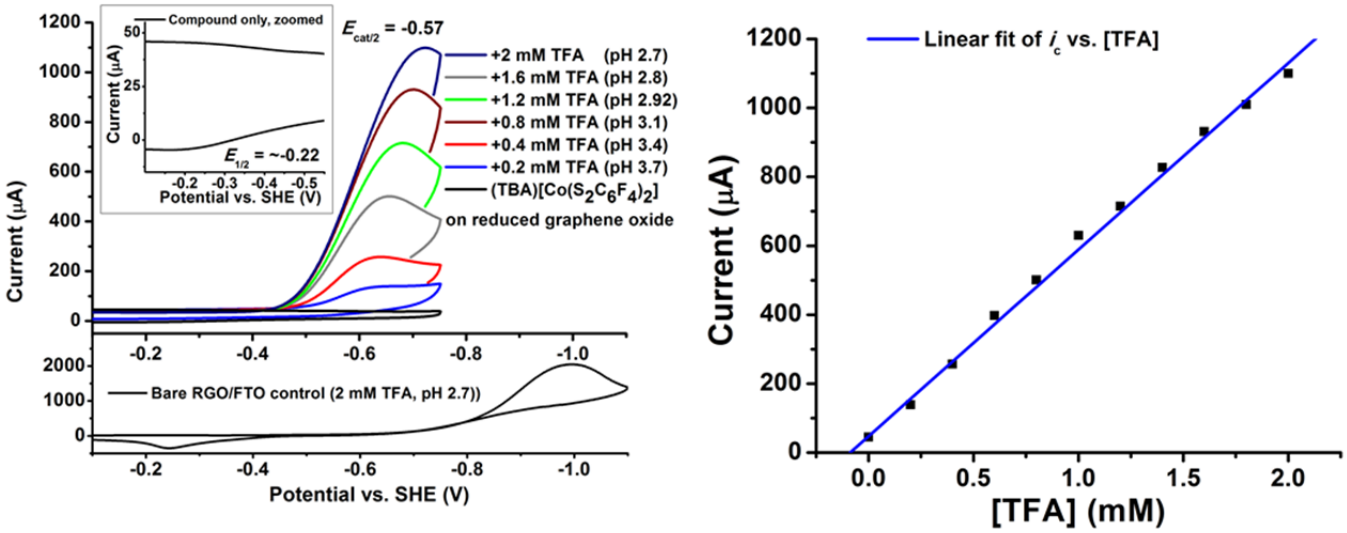

Figure S15. *Left:* Cyclic voltammetry of (TBA)[Co($S_2C_6F_4$)$_2$] (**4**) adsorbed on a **FTO/RGO** working electrode with addition of TFA at a scan rate of 50 mV/s. The control surface (using an FTO/RGO electrode without adsorbed catalyst) under the same conditions is displayed on the bottom of the graph, and the inset provides a zoomed view of the CV of the Co catalyst functionalized surface in the absence of acid. The solution contained 0.1 M aqueous potassium hexafluorophosphate. The counter electrode was a platinum disc, and the reference was an Ag/AgCl (saturated KCl solution) electrode. An equimolar solution of potassium ferricyanide/ferrocyanide (0.5 mM total) was used as an external standard. Potentials are reported versus the standard hydrogen electrode. *Right:* Linear fit of the peak catalytic current versus increasing TFA concentrations, indicating an acid-diffusion controlled process under these conditions.

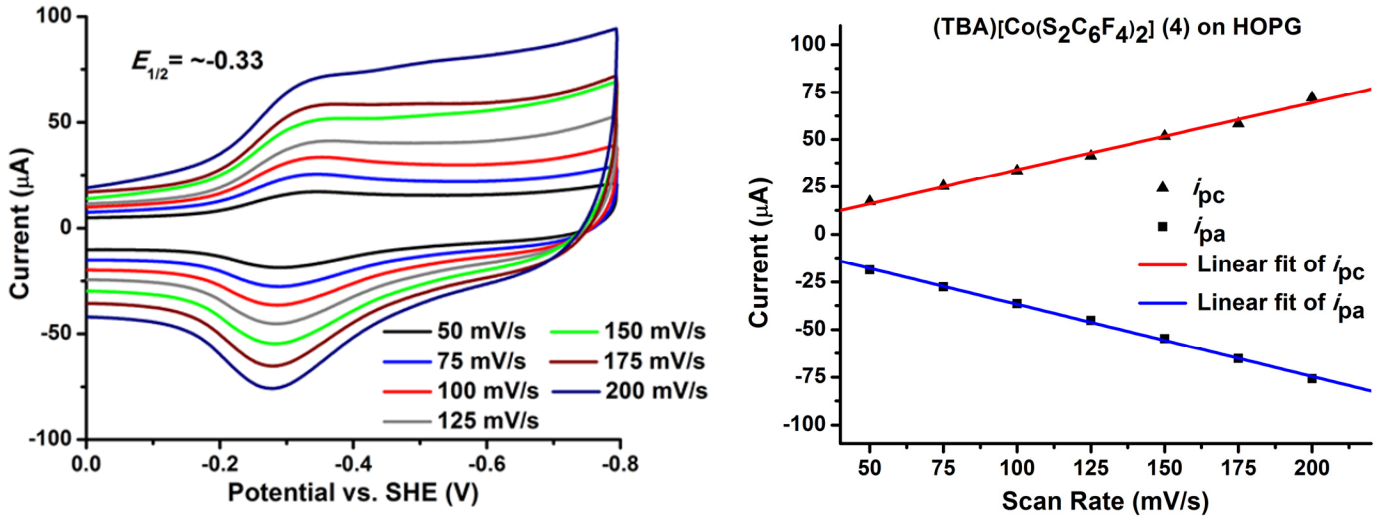

Figure S16. *Left:* Cyclic voltammetry of (TBA)[Co($S_2C_6F_4$)$_2$] (**4**) adsorbed on an **HOPG** working electrode at various scan rates. The solution contained 0.1 M aqueous potassium hexafluorophosphate. The counter electrode was a platinum disc, and the reference was an Ag/AgCl (saturated KCl solution) electrode. An equimolar solution of potassium ferricyanide/ferrocyanide (0.5 mM total) was used as an external standard. Potentials are reported versus the standard hydrogen electrode. *Right:* Linear fit of the peak cathodic and anodic current versus the scan rate.

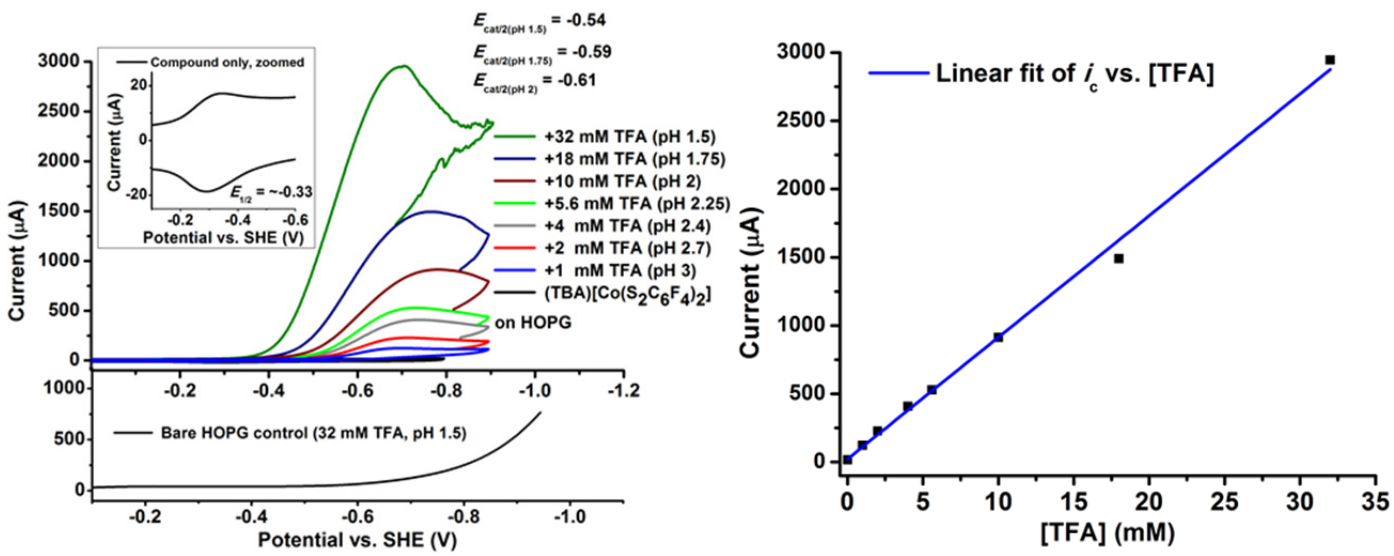

Figure S17. *Left:* Cyclic voltammetry of (TBA)[Co($S_2C_6F_4$)$_2$] (**4**) adsorbed on an **HOPG** working electrode with addition of TFA at a scan rate of 50 mV/s. The control surface (using the same electrode before catalyst soaking) under the same conditions is displayed on the bottom of the graph, and the inset provides a zoomed view of the CV of the Co catalyst functionalized surface in the absence of acid. The solution contained 0.1 M aqueous potassium hexafluorophosphate. The counter electrode was a platinum disc, and the reference was an Ag/AgCl (saturated KCl solution) electrode. An equimolar solution of potassium ferricyanide/ferrocyanide (0.5 mM total) was used as an external standard. Potentials are reported versus the standard hydrogen electrode. *Right:* Linear fit of the peak catalytic current versus increasing TFA concentrations, indicating an acid-diffusion controlled process under these conditions.

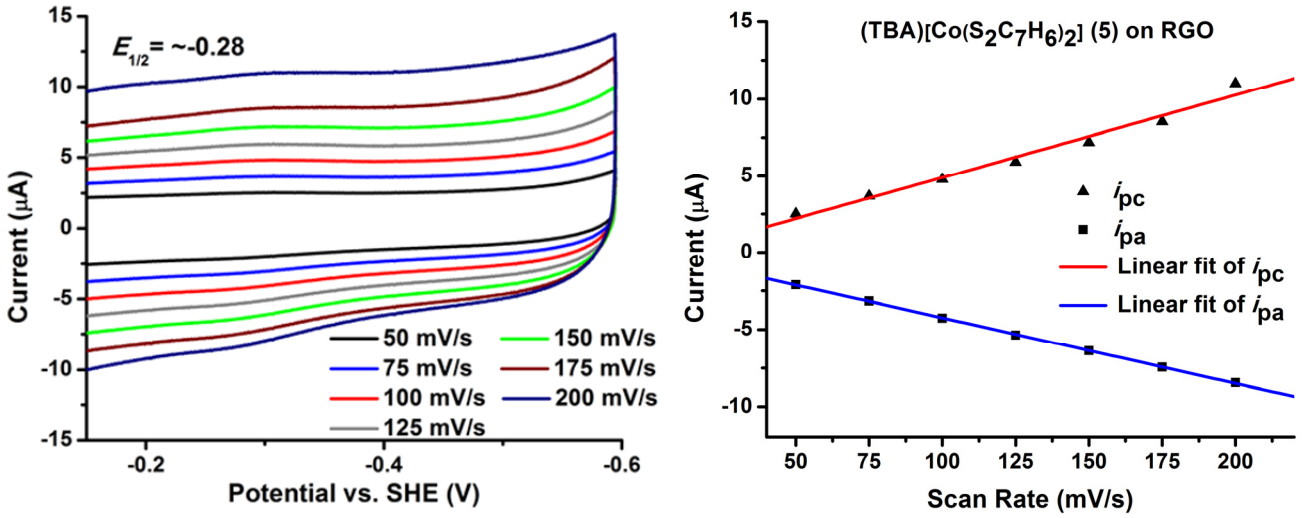

Figure S18. *Left:* Cyclic voltammetry of (TBA)[Co($S_2C_7H_6$)$_2$] (**5**) adsorbed on a **FTO/RGO** working electrode at various scan rates. The solution contained 0.1 M aqueous potassium hexafluorophosphate. The counter electrode was a platinum disc, and the reference was an Ag/AgCl (saturated KCl solution) electrode. An equimolar solution of potassium ferricyanide/ferrocyanide (0.5 mM total) was used as an external standard. Potentials are reported versus the standard hydrogen electrode. *Right:* Linear fit of the peak cathodic and anodic current versus the scan rate.

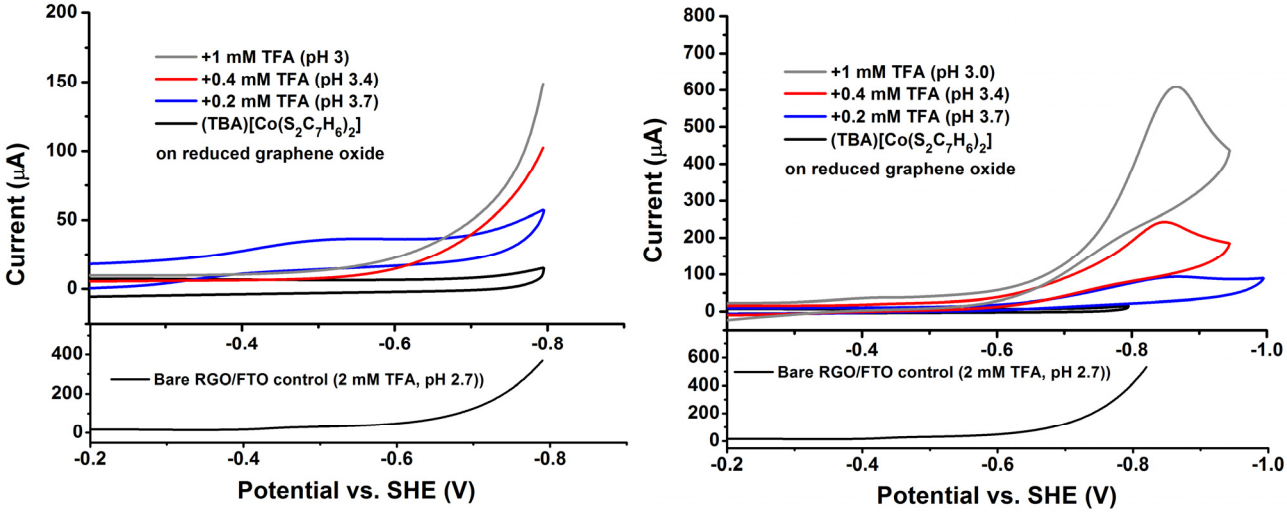

Figure S19. Cyclic voltammetry of (TBA)[Co($S_2C_7H_6$)$_2$] (**5**) adsorbed on two distinct **FTO/RGO** working electrodes with addition of TFA at a scan rate of 50 mV/s. The control surface (using an FTO/RGO electrode without adsorbed catalyst) under the same conditions is displayed on the bottom of the graph. Return (anodic) scans are omitted for clarity in some cases. The solution contained 0.1 M aqueous potassium hexafluorophosphate. The counter electrode was a platinum disc, and the reference was an Ag/AgCl (saturated KCl solution) electrode. An equimolar solution of potassium ferricyanide/ferrocyanide (0.5 mM total) was used as an external standard. Potentials are reported versus the standard hydrogen electrode. *Left:* The electrode exhibits some increase in cathodic current with initial acid addition, but subsequent additions are only seen to produce background current. *Right:* The electrode is only seen to exhibit cathodic current corresponding to background current.

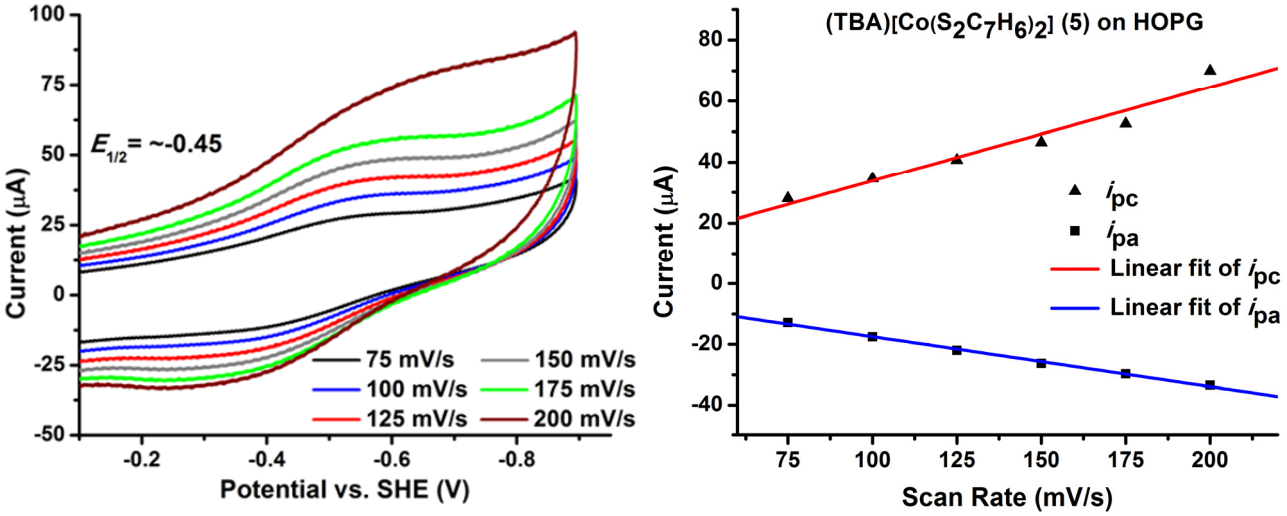

Figure S20. *Left:* Cyclic voltammetry of (TBA)[Co($S_2C_7H_6$)$_2$] (**5**) adsorbed on an **HOPG** working electrode at various scan rates. The solution contained 0.1 M aqueous potassium hexafluorophosphate. The counter electrode was a platinum disc, and the reference was an Ag/AgCl (saturated KCl solution) electrode. An equimolar solution of potassium ferricyanide/ferrocyanide (0.5 mM total) was used as an external standard. Potentials are reported versus the standard hydrogen electrode. *Right:* Linear fit of the peak cathodic and anodic current versus the scan rate.

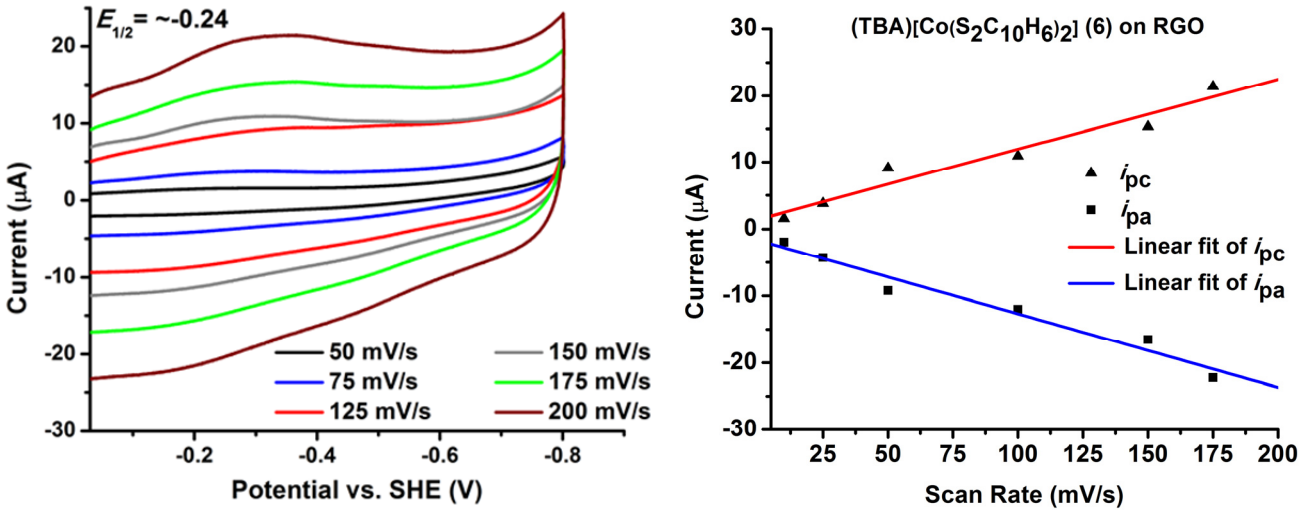

Figure S21. *Left:* Cyclic voltammetry of (TBA)[Co($S_2C_{10}H_6$)$_2$] (**6**) adsorbed on a **FTO/RGO** working electrode at various scan rates. The solution contained 0.1 M aqueous potassium hexafluorophosphate. The counter electrode was a platinum disc, and the reference was an Ag/AgCl (saturated KCl solution) electrode. An equimolar solution of potassium ferricyanide/ferrocyanide (0.5 mM total) was used as an external standard. Potentials are reported versus the standard hydrogen electrode. *Right:* Linear fit of the peak cathodic and anodic current versus the scan rate.

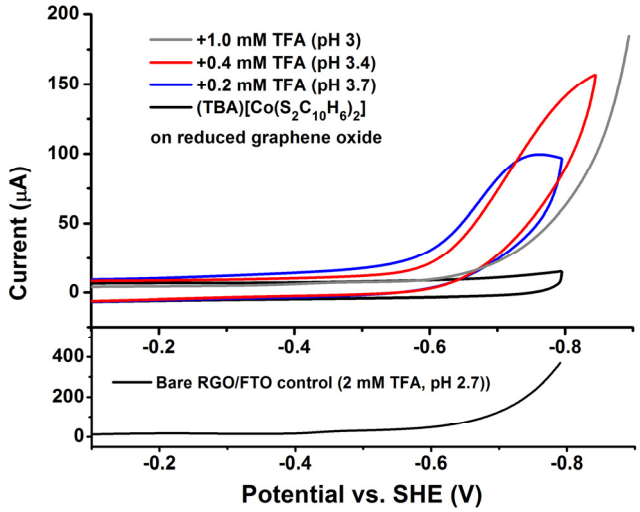

Figure S22. Cyclic voltammetry of (TBA)[Co($S_2C_{10}H_6$)$_2$] (**6**) adsorbed on a **FTO/RGO** working electrode with addition of TFA at a scan rate of 50 mV/s. The control surface (using an FTO/RGO electrode without adsorbed catalyst) under the same conditions is displayed on the bottom of the graph. Return (anodic) scans are omitted for clarity in some plots. The solution contained 0.1 M aqueous potassium hexafluorophosphate. The counter electrode was a platinum disc, and the reference was an Ag/AgCl (saturated KCl solution) electrode. An equimolar solution of potassium ferricyanide/ferrocyanide (0.5 mM total) was used as an external standard. Potentials are reported versus the standard hydrogen electrode. The electrode exhibits some increase in cathodic current with initial acid additions, but subsequent additions are only seen to produce background current.

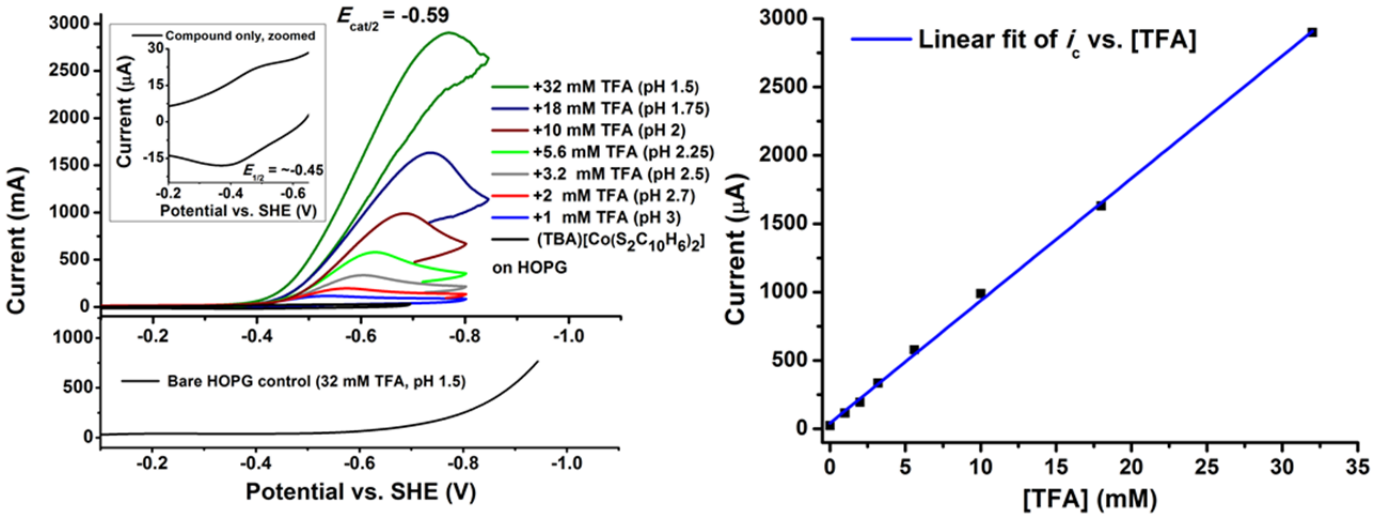

Figure S23. *Left:* Cyclic voltammetry of (TBA)[$Co(S_2C_{10}H_6)_2$] (**6**) adsorbed on an **HOPG** working electrode with addition of TFA at a scan rate of 50 mV/s. The control surface (using the same electrode before catalyst soaking) under the same conditions is displayed on the bottom of the graph, and the inset provides a zoomed view of the CV of the Co catalyst functionalized surface in the absence of acid. The solution contained 0.1 M aqueous potassium hexafluorophosphate. The counter electrode was a platinum disc, and the reference was an Ag/AgCl (saturated KCl solution) electrode. An equimolar solution of potassium ferricyanide/ferrocyanide (0.5 mM total) was used as an external standard. Potentials are reported versus the standard hydrogen electrode. *Right:* Linear fit of the peak catalytic current versus increasing TFA concentrations, indicating an acid-diffusion controlled process under these conditions.

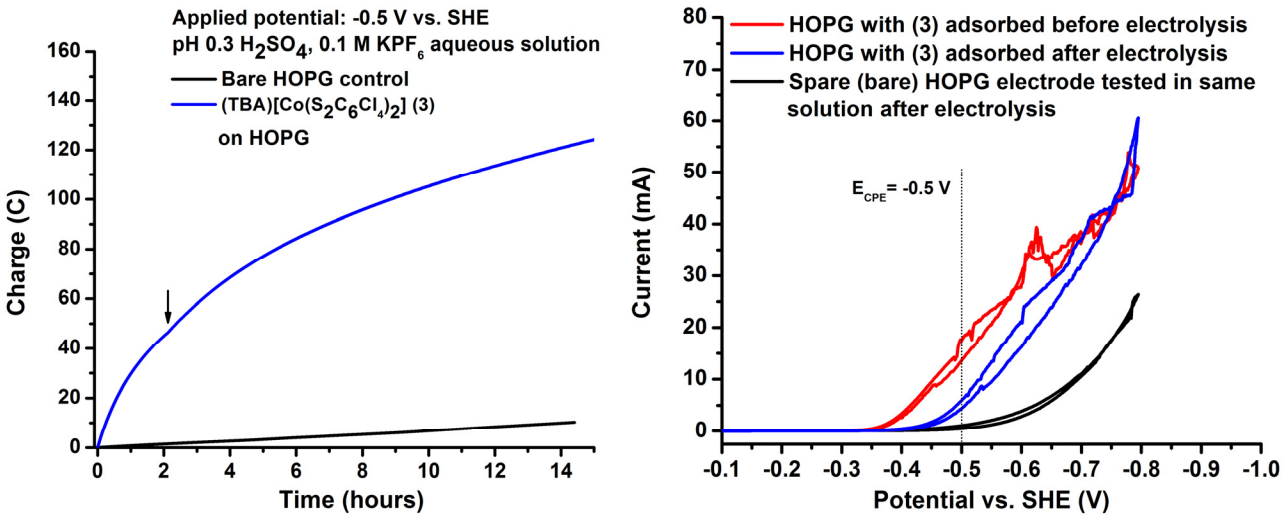

Figure S24. *Left*: Controlled Potential Electrolysis at -0.5 V vs. SHE of (TBA)[$Co(S_2C_6Cl_4)_2$] (**3**) adsorbed on an **HOPG** electrode in an aqueous 0.1 M KPF_6 solution with 0.5 M H_2SO_4 (pH 0.3). A two-compartment cell is used with platinum counter and Ag/AgCl reference electrodes. The arrow indicates when the pH was adjusted back to 0.3. *Right*: Cyclic voltammograms of the electrolysis setup in situ before (red trace) and after (blue trace) the CPE experiment. A separate bare HOPG working electrode was tested in the solution after electrolysis (black trace) to confirm residual catalytic current was present after electrolysis. The abnormal shapes of the cathodic waves are both due to the diffusion conditions (stirring) in the cell and due to the dihydrogen bubbles generated at the working electrode.

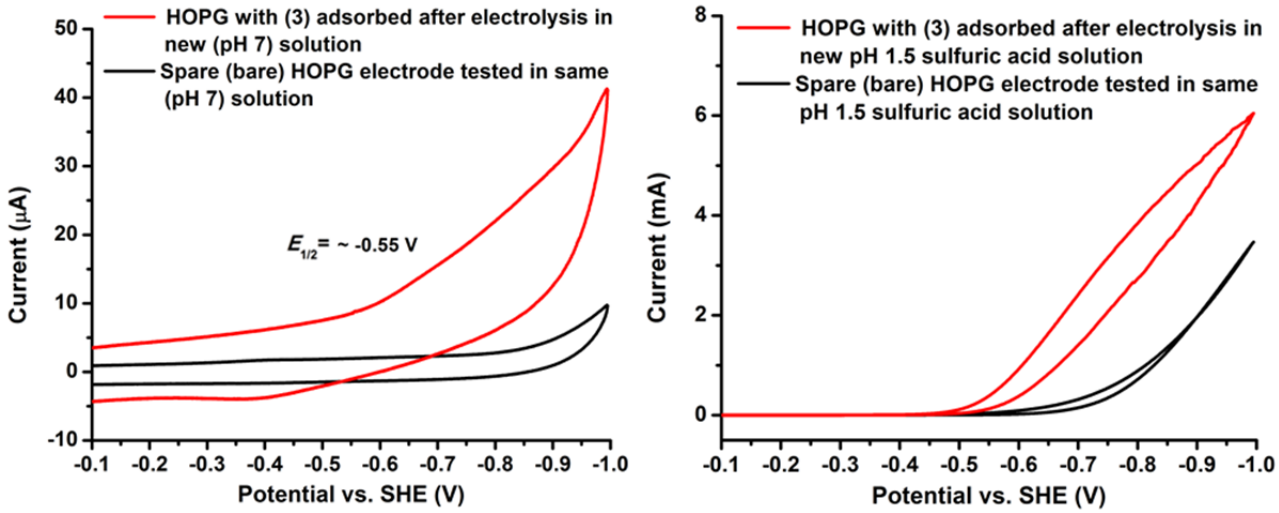

Figure S25. *Left*: Cyclic voltammogram of (TBA)[Co($S_2C_6Cl_4$)$_2$] (**3**) adsorbed on an **HOPG** electrode (red trace) after CPE experiment in a new (pH 7) aqueous 0.1 M KPF_6 solution. A separate (bare) HOPG electrode tested in the same solution (black trace) is provided for comparison. *Right*: Cyclic voltammogram of (TBA)[Co($S_2C_6Cl_4$)$_2$] (**3**) adsorbed on an HOPG electrode (red trace) after CPE experiment in a new solution with sulfuric acid added to reach pH 1.5, showing residual catalytic activity in the new solution. A separate (bare) HOPG electrode tested in the same solution (black trace) is provided for comparison.

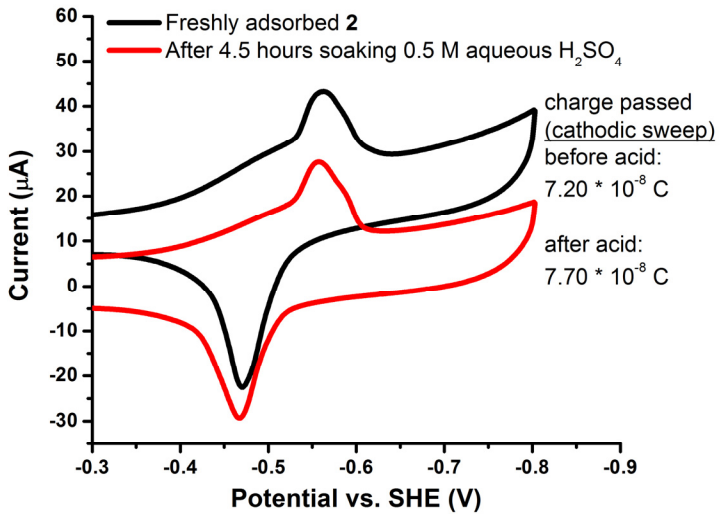

Figure S26. Cyclic voltammogram of (TBA)[Co($S_2C_6Cl_2H_2$)$_2$] (**2**) adsorbed on an **HOPG** electrode disc before (black trace) and after (red trace) soaking in an 0.5 M H_2SO_4 solution (pH 0.3) for 4 hours. Integration of the cathodic peak current shows a change in charge equal to less than 10% of the total charge, which can be attributed to the error of CV integration for quantification. The higher catalyst loading of **2** compared to **Figure S9** is due to the higher geometric surface area exposed to solution for the HOPG disc, as well as the higher roughness of the electrode without extended polishing (used here to increase catalyst loading for better comparison). The two cathodic responses that are apparent in the current response have been commonly observed in our previous reports for bulk graphite,[1] likely due to the exposure of the catalyst to multiple graphite planes in the rough, unpolished HOPG disk, giving rise to multiple catalyst orientations which results in slightly different observed reduction potentials. Cyclic voltammograms were run at 50 mV/s in a pH 7 aqueous 0.1 M KPF_6 solution. The counter electrode was a platinum disc, and the reference was an Ag/AgCl (saturated KCl solution) electrode.

4. Determination of Catalytic Turnover Frequencies

The proton reduction activity rate constants for the FTO/RGO- and HOPG-adsorbed catalyst systems were assessed (a) by methods reported by Kubiak et al. and used for similar heterogenized molecular catalysts (**equation 1**)[2,3] and (b) by the analysis of bulk electrolysis performance.

Cyclic voltammetry acid titrations

For both FTO/RGO- and HOPG-adsorbed systems acid concentrations used for analysis were below the maximum activity levels (activity saturation), in the FTO/RGO system due to the substantial tin oxide reduction seen at high acid concentrations, and in the HOPG system due to disruption of the voltammogram signals by H_2 production at high acid concentrations (see **Figure 3**, bottom left, as example) as well as background acid reduction at graphite under these conditions. Rates predicted by this method are thus expected to be an underestimate of the *maximum* TOF at acid saturation.

(1) $$\boldsymbol{k_{obs}} = \frac{\boldsymbol{i}_{\mathrm{cat}}}{\boldsymbol{nFA\Gamma}}$$

Here, i_{cat} is the catalytic current at pH 1.5, n is the number of redox equivalents transferred during the HER, F is the Faraday constant, A is the geometric surface area of the HOPG electrode (0.2 cm^2) and Γ is the catalyst loading as determined by voltammetry in the absence of acid (see Table 1).

For the HOPG/**3** system, analysis in the presence of trifluoroacetic acid at a concentration of 32 mM (pH 1.5) gives an i_{cat} value of 2,818 μA, and is predicted by **equation 1** to have a rate constant of 120 s^{-1} based on a catalyst loading of 6.22 x 10^{-10} mol/cm^2 calculated by CV integration. In the HOPG/**1** system, activity saturation is observed at an acid concentration of only 9 mM TFA (pH ~2); therefore, the i_{cat} value of 224 μA determined at this pH was used with the catalyst loading of 2.70 x 10^{-11} mol/cm^2 to calculate a k_{obs} of 220 s^{-1}.

Bulk electrolysis

Only HOPG-adsorbed catalysts were analyzed by bulk electrolysis due to the limited stability of the FTO electrodes to reductive bias in acidic solutions. To determine TOF values based on electrolysis data, the cutoff point for turnover is selected as the time the current reaches a plateau current, after which no significant decrease of the slope in the current vs. time graph is observed. The TON is then calculated as the total amount of dihydrogen generated by the cutoff point (current passed/electrons required for HER) divided by the catalyst loading found by CV integration prior to electrolysis. The average TOF is calculated as the TON divided by the time to reach the cutoff point, while the initial TOF is calculated based on the total current drawn in the first 30 minutes, using the same catalyst loading.

For the HOPG/**3** system, the cutoff point is selected to be 8 hours, corresponding to a total of 96 C or 9.95 x 10^{-4} moles of electrons passed and approximately 5 x 10^{-4} moles of dihydrogen formed. Based on a catalyst loading of 6.22 x 10^{-10} mol/cm^2, a TON of 4.02 x 10^6 is calculated (after 8 hours), with an average TOF of 140 s^{-1} over the 8 hour period.

5. X-ray Crystallography

Table S1. Crystal data and structure refinement for **6**.

Identification code	see
Empirical formula	C36 H48 Co N S4
Formula weight	681.92
Temperature	85(2) K
Wavelength	1.54178 A
Crystal system, space group	Monoclinic, C2/c
Unit cell dimensions	a = 22.0233(10) A alpha = 90 deg. b = 8.3802(2) A beta = 104.229(13) deg. c = 19.1932(15) A gamma = 90 deg.
Volume	3433.6(4) A^3
Z, Calculated density	4, 1.319 Mg/m^3
Absorption coefficient	6.375 mm^-1
F(000)	1448
Crystal size	0.09 x 0.03 x 0.01 mm
Theta range for data collection	4.142 to 69.642 deg.
Limiting indices	-26<=h<=26, -10<=k<=10, -23<=l<=22
Reflections collected / unique	25589 / 3213 [R(int) = 0.1651]
Completeness to theta = 67.679	99.9 %
Absorption correction	Semi-empirical from equivalents
Max. and min. transmission	1.00000 and 0.62259
Refinement method	Full-matrix least-squares on F^2
Data / restraints / parameters	3213 / 0 / 194
Goodness-of-fit on F^2	1.114
Final R indices [I>2sigma(I)]	R1 = 0.0806, wR2 = 0.2126
R indices (all data)	R1 = 0.0949, wR2 = 0.2567
Extinction coefficient	n/a
Largest diff. peak and hole	1.107 and -1.478 e.A^-3

6. References

(1) Eady, S. C.; MacInnes, M. M.; Lehnert, N. A Smorgasbord of Carbon: Electrochemical Analysis of Cobalt–Bis(benzenedithiolate) Complex Adsorption and Electrocatalytic Activity on Diverse Graphitic Supports *ACS Appl. Mater. Interfaces* **2016**, *8*, 23624.

(2) Sathrum, A. J.; Kubiak, C. P. Kinetics and Limiting Current Densities of Homogeneous and Heterogeneous Electrocatalysts *J. Phys. Chem. Lett.* **2011**, *2*, 2372.

(3) Das, A. K.; Engelhard, M. H.; Bullock, R. M.; Roberts, J. A. S. A Hydrogen-Evolving $Ni(P_2N_2)_2$ Electrocatalyst Covalently Attached to a Glassy Carbon Electrode: Preparation, Characterization, and Catalysis. Comparisons with the Homogeneous Analogue *Inorg. Chem.* **2014**, *53*, 6875.